Journal of Non-Crystalline Solids 650 (2025) 123382

Contents lists available at ScienceDirect

Journal of Non-Crystalline Solids

journal homepage: www.elsevier.com/locate/jnoncrysol

Improvement of soft magnetic properties for Fe-based amorphous/nanocrystalline alloy by longitudinal magnetic field annealing

Mufeng Jiang [a], Jingjing Wang [a], Mingjuan Cai [a,b], Jun Li [a], Wanying Dong [a], Zhijun Guo [a,*], Baolong Shen [a,*]

[a] School of Materials Science and Engineering, Jiangsu Key Laboratory of Advanced Metallic Materials, Southeast University, Nanjing 211189, China
[b] Anhui Province Key Laboratory of Low-Energy Quantum Materials and Devices, High Magnetic Field Laboratory, HFIPS, Chinese Academy of Sciences, Hefei 230031, China

ARTICLE INFO

Keywords:
Magnetic field annealing
Co substitution
Amorphous matrix
Nanocrystalline
Soft magnetic properties
Magnetic domains

ABSTRACT

This study investigated the enhancement of soft magnetic properties in $Fe_{83.2-x}Co_xSi_{2.5}B_{9.5}P_4Cu_{0.8}$ ($x = 0$, 4, 8, 12 and 16 at %) amorphous/nanocrystalline alloys through longitudinal magnetic field annealing (FA). The FA-treated alloys demonstrate superior magnetic performance, achieving a superior saturation flux density (B_s) of 1.85 T, ultra-low coercivity (H_c) of 1.8 A/m, high effective permeability (μ_e) of 26,505 at 1 kHz, and low core loss (0.13 W/kg) at 1.0 T/50 Hz. Microstructural analysis reveals that the FA and Co substitution promotes nanocrystalline nucleation, forming high-density nanocrystals while suppressing grain growth through competitive dynamics and inhibiting element diffusion within the amorphous matrix. Domain observation further confirms that FA facilitates the transition from disordered, non-uniform magnetic to uniform, broad, plate-like domains. These findings elucidate the critical influence of longitudinal magnetic field annealing on microstructure evolution and magnetic domain alignment, which synergistically enhance soft magnetic properties.

1. Introduction

The demand for advanced soft magnetic materials with maximized saturation magnetic flux density (B_s) and minimization coercivity (H_c) has become increasingly critical in modern power electronics, including inductors and electric motors, to achieve high efficiency, miniaturization and energy saving [1–3]. Since the discovery of magnetic induction by Michael Faraday, materials such as silicon steel [4], permalloys [5], soft ferrites [6], and amorphous or nanocrystalline alloys [7,8] have been extensively developed to meet these requirements. Among these, Fe-based amorphous/nanocrystalline alloys stand out due to their unique composite microstructure comprising nano-sized α-Fe crystals uniformly embedded within an amorphous matrix. This structure enables strong intergranular exchange coupling, which suppresses magnetocrystalline anisotropy, while the opposing magnetostriction contributions from the α-Fe and amorphous phases yield near-zero magnetostriction, resulting in exceptional soft magnetic properties [9,10].

Despite these advantages, achieving an optimal balance between high B_s and low H_c remains challenging. Alloy design strategies often involve heavy doping with non-magnetic elements to enhance amorphous-forming ability (AFA) and nucleation sites while restricting grain growth, thereby reducing H_c. However, these strategies can also dilute the ferromagnetic component, limiting the achievable B_s [11,12]. Co-doping has emerged as a promising solution to enhance B_s without compromising manufacturability [13–16]. Yet, excessive Co content increases magnetic anisotropy, which cannot be sufficiently averaged through exchange interactions, thereby increasing H_c and degrading magnetic softness [16,17]. Field annealing has been identified as a powerful approach to mitigate the adverse effects of Co substitution by inducing uniaxial magnetic anisotropy with an easy axis aligned along the applied field direction [18,19]. However, previous studies have largely focused on amorphous alloys, with a limited understanding of the structural transformation and magnetic performance of nanocrystalline alloys under Field annealing[20].

This study systematically investigates the effects of FA treatment and Co substitution on the microstructure, magnetic domain structure, and soft magnetic properties of $Fe_{83.2-x}Co_xSi_{2.5}B_{9.5}P_4Cu_{0.8}$ alloys. Our findings demonstrate that FA treatment significantly improves soft magnetic properties, particularly in alloys with Co content $x \geq 8$. Notably, the

* Corresponding authors.
E-mail addresses: zj-guo@seu.edu.cn (Z. Guo), blshen@seu.edu.cn (B. Shen).

https://doi.org/10.1016/j.jnoncrysol.2024.123382
Received 2 December 2024; Received in revised form 22 December 2024; Accepted 25 December 2024
Available online 6 January 2025

$Fe_{67.2}Co_{16}Si_{2.5}B_{9.5}P_4Cu_{0.8}$ alloy exhibits a remarkable B_s of 1.85 T, an ultra-low H_c of 1.8 A/m, and a high μ_e of 26,505 at 1 kHz after FA treatment under 0.1 T magnetic field. TEM analysis reveals that FA promotes fine nanocrystalline nucleation and suppresses grain growth, while magneto-optical Kerr microscopy shows that the magnetization mechanism shifts from non-uniform domain rotation to uniform domain wall displacement. This work provides valuable insights into the development of next-generation soft magnetic nanocrystalline alloys with low losses and high magnetic performance, suitable for energy-efficient applications.

2. Experimental methods

Multicomponent alloy ingots with the nominal atomic compositions of $Fe_{83.2-x}Co_xSi_{2.5}B_{9.5}P_4Cu_{0.8}$($x$ = 0, 4, 8, 12, 16) were prepared with pure materials of Fe (99.99 wt.%), Co (99.99 wt.%), Si (99.999 wt.%), B (99.9 wt.%), Cu (99.99 wt.%) and before alloy of FeP (consisting of 73.6 wt.% Fe and 26.4 wt.% P). Induction melting was performed under an argon atmosphere, ensuring mass losses of <0.2 wt.%. Rapid solidification into as-quenched (AQ) ribbon samples was achieved *via* single-roller melt-spinning (roller speed: 40 m/s; pressure differential: 0.015–0.02 MPa), also under an argon atmosphere. The resulting ribbons were approximately 1 mm in width and 23 μm in thickness. The ribbons were subsequently sectioned into 6 mm lengths and subjected to isothermal annealing at various temperatures ranging from 420 to 560 °C to promote nanocrystallization. The annealing protocol involved the following steps: (1) encapsulation of ribbon specimens in quartz tubes under a vacuum atmosphere (5 $\times 10^{-3}$ Pa); (2) immersion of the sealed tubes into preheated furnaces maintained at target annealing temperatures, with a dwell time of 3 min; (3) rapid quenching of the tubes in water to ambient temperature. Annealing treatments were performed both in the absence of an applied magnetic field (NA) and with a longitudinal magnetic field of 0.1 T applied along the ribbon axis (FA). The AQ, NA, and FA-treated $Fe_{83.2-x}Co_xSi_{2.5}B_{9.5}P_4Cu_{0.8}$($x$ = 0, 4, 8, 12, 16) ribbons are hereafter designated as Cox-AQ, Co_x-NA, and Co_x-FA, respectively.

The microstructural characterization of the ribbons was carried out using X-ray diffraction (XRD) on a Bruker D8 Discover diffractometer with Cu-Kα radiation and transmission electron microscopy (TEM, JEM-2000EX). Thermal analysis was performed using a differential scanning calorimeter (DSC, NETZSCH 404 F3) under high-purity argon flow, employing a heating rate of 0.67 K/s. Magnetic properties, including B_s and H_c, were evaluated using a vibrating sample magnetometer (VSM, Lake Shore 7410) under a maximum applied field of 800 kA/m and a B-H loop tracer (RIKEN BHS-40) under a field of 1 kA/m, respectively. The μ_e was measured with an Agilent 4294A impedance analyzer under a field strength of 5 A/m. Magnetic domain structures were visualized via magneto-optical Kerr microscopy (Evico Magnetics GmbH, em-Kerr-highres). All reported magnetic measurements represent the mean of three independent specimens for each alloy composition to ensure reproducibility and statistical rigor.

3. Results and discussion

The XRD patterns of AQ $Fe_{83.2-x}Co_xSi_{2.5}B_{9.5}P_4Cu_{0.8}$ (x = 0, 4, 8, 12, 16) ribbons, as presented in Fig. 1, confirm the predominantly amorphous nature of these alloys. Across all compositions, the absence of sharp diffraction peaks indicative of crystallinity, coupled with the presence of broad humps characteristic of the amorphous phase, suggests that the rapid solidification process effectively suppresses long-range atomic ordering. This observation implies that the introduction of Co as a partial replacement for Fe does not adversely impact the alloy's AFA, even at higher Co concentrations.

The thermal behavior of the AQ $Fe_{83.2-x}Co_xSi_{2.5}B_{9.5}P_4Cu_{0.8}$ ribbons was analyzed through DSC, as depicted in Fig. 2. Each DSC curve exhibits two distinct exothermic peaks, corresponding to sequential

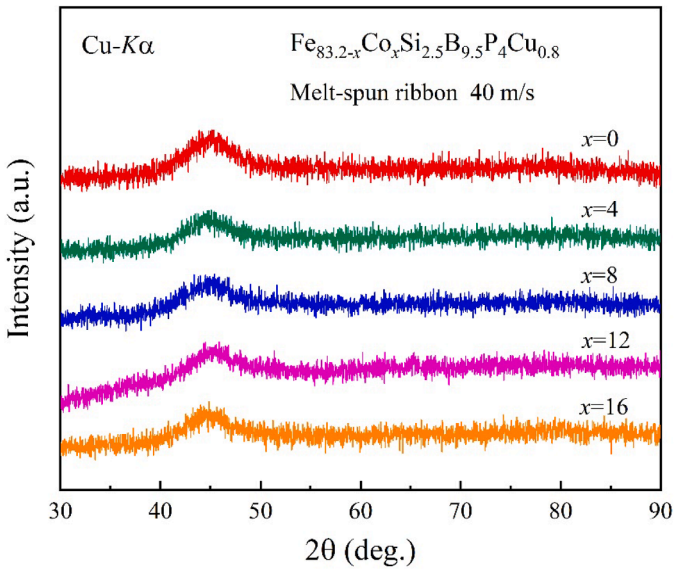

Fig. 1. XRD patterns of $Fe_{83.2-x}Co_xSi_{2.5}B_{9.5}P_4Cu_{0.8}$ (x = 0, 4, 8, 12, 16) ribbons in AQ state.

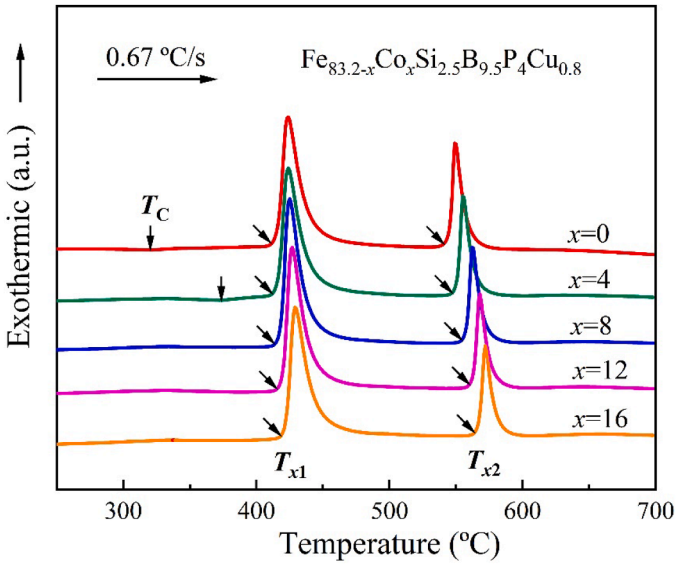

Fig. 2. DSC curves of $Fe_{83.2-x}Co_xSi_{2.5}B_{9.5}P_4Cu_{0.8}$ (x = 0, 4, 8, 12, 16) ribbons in AQ state.

crystallization events. The first exothermic peak, appearing at a lower temperature, is associated with the primary crystallization of α-Fe(Co) phases, while the second peak at higher temperatures corresponds to the precipitation of (Fe, Co)-metalloid compounds. With increasing Co content from x = 0 to 16, both the primary crystallization temperature (T_{x1}) and the secondary crystallization temperature (T_{x2}) shift progressively to higher temperatures. This trend results in an expansion of the crystallization temperature interval ($\Delta T_x = T_{x2} - T_{x1}$) from 129 °C to 145 °C, indicating that Co substitution enhances the thermal stability of the alloy system. The broader promotes more controlled nucleation of the α-Fe(Co) phase while suppressing the early formation of secondary phases, which is advantageous for achieving superior soft magnetic properties. Furthermore, the Curie temperature (T_C) can be discerned only for the Co_0-AQ and Co_4-AQ samples, with values of 316 °C and 374 °C, respectively. For samples with higher Co concentrations, no discernible magnetic transition is observed within the measured range, suggesting that the T_C exceeds T_{x1}. These thermal insights informed the

selection of annealing temperatures for subsequent FA and NA treatments, which were conducted between 420 and 560 °C for 3 min to promote nanocrystalline phase development.

The FA and NA treatments have different impacts on the soft-magnetic properties of ribbon samples with different Co contents. Fig. 3 illustrates the H_c, μ_e and B_s of $Fe_{83.2-x}Co_xSi_{2.5}B_{9.5}P_4Cu_{0.8}$ ($x = 0$, 4, 8, 12, 16) in AQ state and after NA and FA treatments. The specific values are listed in Table 1. Across all compositions, FA-treated samples exhibit markedly lower coercivity, ranging between 1.8 and 4.5 A/m, and significantly higher μ_e values compared to both AQ and NA-treated counterparts. This reduction in H_c is especially pronounced for alloys with $x > 8$, where FA treatment provides a substantial improvement in magnetic softness, particularly for the $x = 16$ composition. As shown in Fig. 3(b), NA treatment induces an initial increase of μ_e, however, the extent of improvement diminishes with increasing Co content. Notably, for the $x = 16$ alloy, NA treatment results in a deterioration of μ_e, underscoring the limits of this approach in high-Co-content systems. In contrast, FA treatment consistently enhances μ_e, with values reaching as high as 26,505, indicating the superior effectiveness of FA in promoting magnetic softness across all compositions. The dependence of B_s on Co content, **shown in** Fig. 3(c), reveals a steady increase in B_s for FA-treated samples, rising from 1.77 T to 1.85 T as the Co content increases. This trend aligns with the increase in the average magnetic moment, which can be attributed to the magnetic valence theory [21], as well as the strong ferromagnetic coupling between Fe and Co atoms [22]. These results highlight the critical role of FA treatment in optimizing the soft magnetic properties of Fe-Co-based alloys, especially at higher Co concentrations, by enhancing both permeability and saturation flux density while minimizing coercivity.

A loss analysis was conducted for the optimal NA and FA samples of Co0, Co8, and Co16 alloys at 50 Hz and 1 kHz, with the results shown in Fig. 4. For alloys with varying Co content, the FA samples (dashed lines) consistently demonstrated lower losses than the NA samples (solid lines) at different magnetic flux densities. Notably, Co16 alloy exhibited a more significant reduction in losses after longitudinal magnetic field heat treatment, which aligns with the change in coercivity shown in

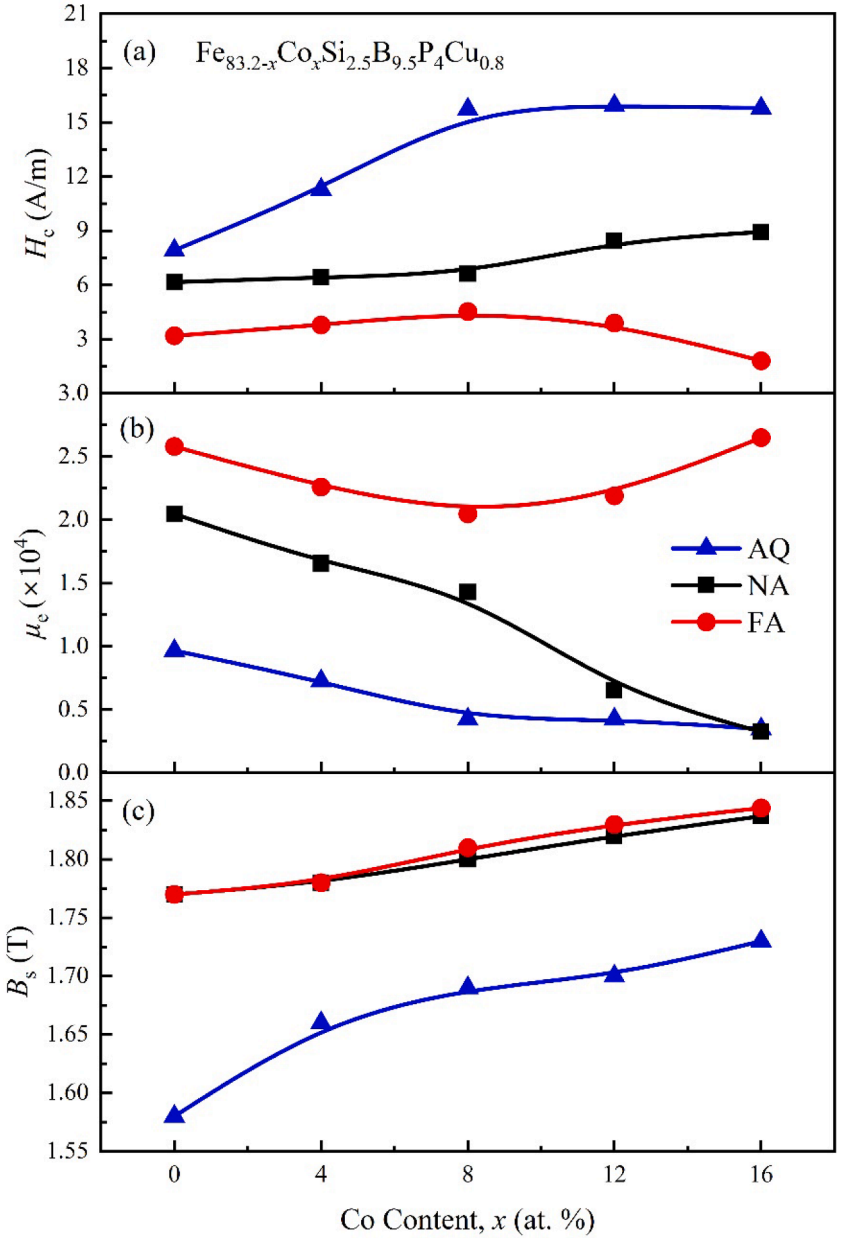

Fig. 3. Changes in (a) H_c, (b) μ_e and (c) B_s as a function of Co content for samples at AQ state and subjected to NA and FA treatment at optimal conditions.

Table 1
Magnetic properties of $Fe_{83.2-x}Co_xSi_{2.5}B_{9.5}P_4Cu_{0.8}$($x$ = 0, 4, 8, 12,16 at %) alloys subjected to optimal NA and FA treatments as well as in AQ state.

Alloys	H_c (A/m)			μ_e			B_s (T)		
	AQ	NA	FA	AQ	NA	FA	AQ	NA	FA
Co 0	7.9	6.2	3.2	9659	20,478	25,810	1.58	1.77	1.77
Co 4	11.3	6.4	3.8	7273	16,562	22,605	1.66	1.78	1.78
Co 8	15.7	6.6	4.5	4250	14,296	20,478	1.69	1.80	1.81
Co 12	15.9	8.4	3.9	4249	6515	21,905	1.70	1.82	1.83
Co 16	15.8	8.9	1.8	3477	3245	26,505	1.73	1.84	1.85

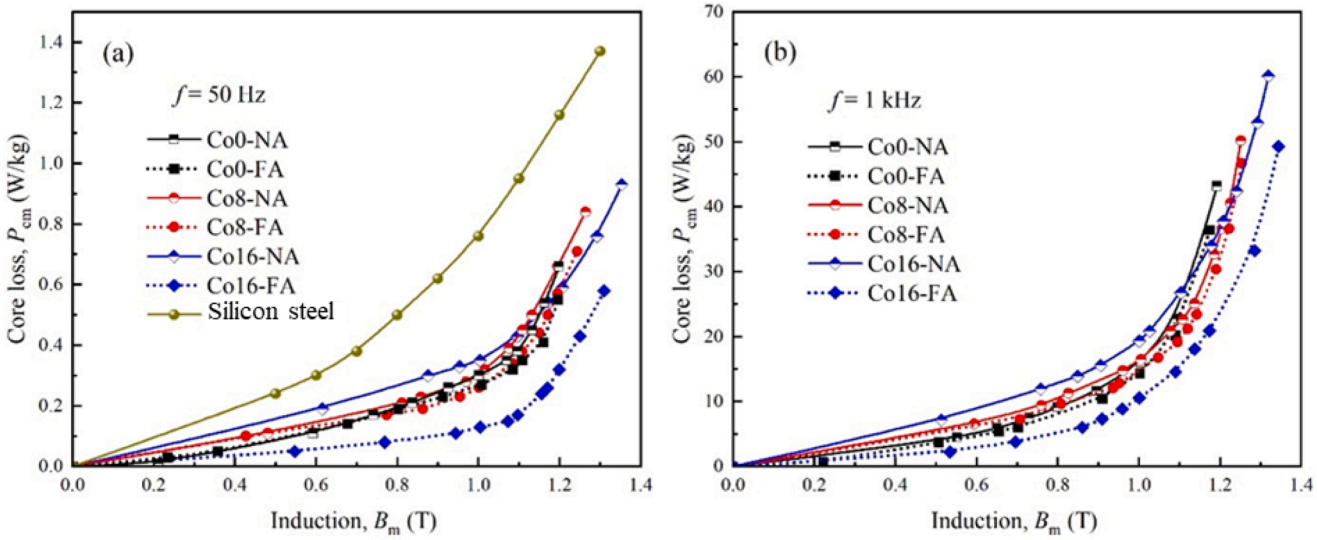

Fig. 4. The dependence of core loss on induction at (a) 50 Hz and (b) 1 kHz for $Fe_{83.2-x}Co_xSi_{2.5}B_{9.5}P_4Cu_{0.8}$ (x = 0, 8, 16) alloys after NA and FA (comparison sample: non-oriented silicon steel [1]).

Fig. 3. At 50 Hz, the FA sample of the Co16 alloy exhibited the lowest loss, with a loss of only 0.13 W/kg under an external field of 1 T—approximately 63 % lower than that of the NA sample and well below the loss values of currently widely used soft magnetic materials: silicon steel. These results highlight the synergy between Co substitution and FA treatment in optimizing the magnetic softness and thermal stability of the alloys.

To evaluate the performance of obtained samples, B_s and H_c values of Co_{16}-FA alloy are compared with other typical Fe-based nanocrystalline alloys (Fe content > 80 at.%) reported in the literature [23–52], as shown in Fig. 5. The Co_{16}-FA alloy, represented by the red star, demonstrates an exceptional balance of high saturation flux density and low coercivity, positioning it favorably relative to other alloy systems, including FeSiBPCu, FeB, and FeBCu-based alloys. This advantageous combination of magnetic properties makes the FeSiBPCu-Co alloy prepared through FA treatment as an outstanding candidate for next-generation industrial applications, such as energy-efficient transformers and motors. Its ability to outperform conventional soft magnetic materials reinforces its relevance for applications where both high magnetic performance and low energy losses are critical.

As the soft-magnetic properties of nanocrystalline alloys are strongly influenced by their microstructure, further analysis was conducted using TEM. Fig. 6 presents bright-field TEM images, selected area electron diffraction (SAED) patterns, and elemental distribution maps for Co_{16}-FA and Co_{16}—NA alloys, annealed at 500 °C for 3 min. Both alloys exhibit a typical amorphous-nanocrystalline structure, but notable differences are observed in the size, distribution, and homogeneity of the nanocrystalline. For the Co_{16}-FA alloy, nanocrystals are primarily distributed in an amorphous matrix within the 7–19 nm range, with an average size of 12 nm (Fig. 6**(a-c)**). In contrast, the Co_{16}-NA alloy shows a broader nanocrystal size range, between 8 and 56 nm, with an average

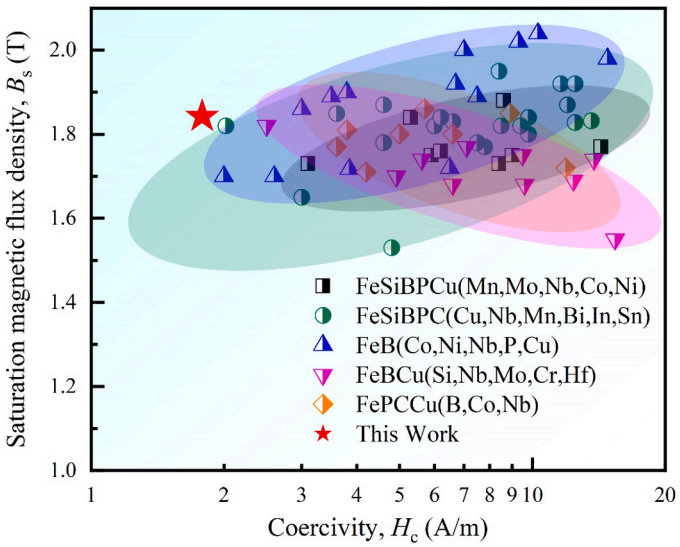

Fig. 5. A summary of B_s and H_c of the Fe-based amorphous/nanocrystalline alloy prepared in this word and other typical high Fe content (> 80 at.%) nanocrystalline alloys [23–52].

size of 29 nm (Fig. 6**(e–g)**). This indicates that the FA-treated alloy develops smaller, more uniformly distributed nanocrystals with a higher crystallization volume fraction. These microstructural differences align with the slightly enhanced B_s, significantly increased μ_e and decreased H_c values observed for Co_{16}-FA in Fig. 3(c), reflecting improved soft-magnetic performance. Elemental distribution analysis further reveals

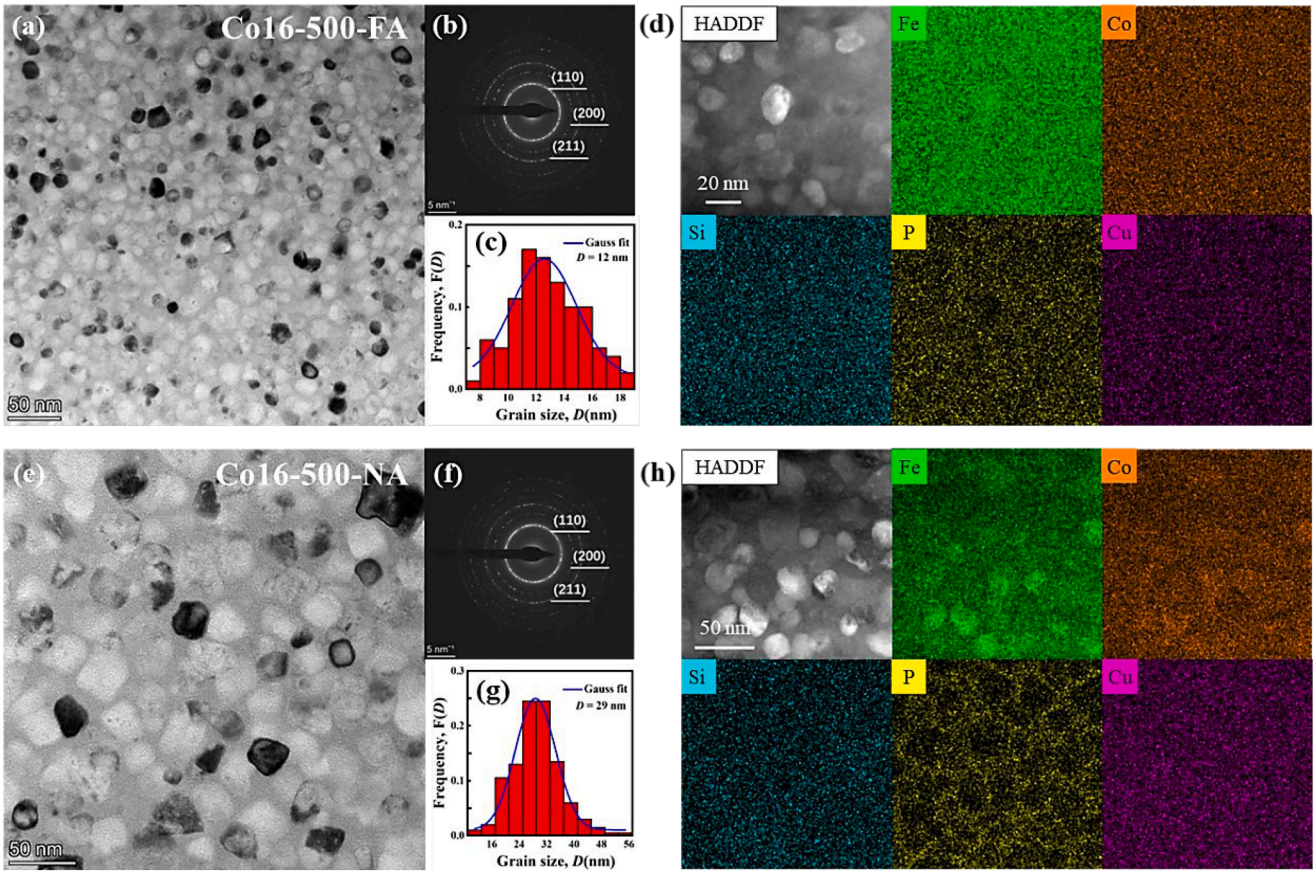

Fig. 6. FA sample with (a) TEM image, (b) SAED pattern, (c) grain size distribution, (d) element distribution and NA sample with (e) TEM image, (f) SAED pattern, (g) grain size distribution, (h) element distribution of $Fe_{67.2}Co_{16}Si_{2.5}B_{9.5}P_4Cu_{0.8}$ alloy annealed at 500℃ for 3 min.

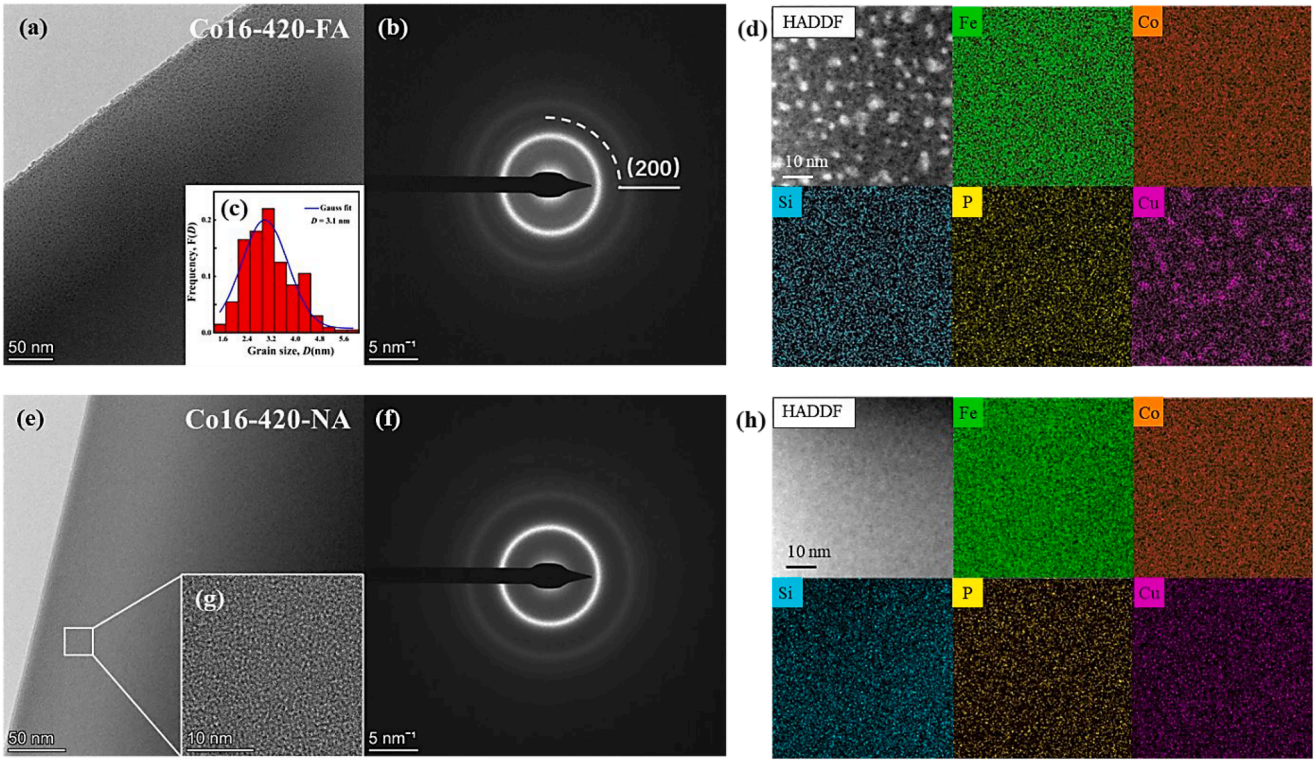

Fig. 7. FA sample with (a) TEM image, (b) SAED pattern, (e) grain size distribution, (d) element distribution and NA sample with (e) TEM image and (g) local enlarged image, (f) SAED image, (h) grain size distribution map of $Fe_{67.2}Co_{16}Si_{2.5}B_{9.5}P_4Cu_{0.8}$ alloy annealed at 420 ℃ for 3 min.

that the Co_{16}-FA alloy exhibits a more homogeneous element distribution compared to the Co_{16}-NA alloy (Fig. 6(h)). Fe and Co elements tend to cluster within the α-Fe(Co) nanocrystalline phase, while P is enriched in the amorphous matrix surrounding these nanocrystals in the NA-treated alloy. This elemental segregation in Co_{16}-NA arises from the diffusion-driven growth of nanocrystals into the surrounding amorphous matrix. In contrast, the Co_{16}-FA alloy exhibits minimal elemental segregation, suggesting more uniform short-range fluctuations and a more stable microstructure. These observations highlight the critical role of FA treatment in promoting finer, more uniform nanocrystallization and reducing elemental segregation, which contributes to the superior magnetic properties of the Co16 -FA alloy.

To elucidate the formation of high-density nanocrystalline in the FA-treated sample, Fig. 7 compares the microstructure of Co_{16}-NA and Co_{16}-FA alloy samples annealed near T_{x1} at 420℃ for 3 min. In the Co_{16}-FA alloy sample, the precipitation of a fine secondary phase is evident, with an average size of 3.1 nm (Fig. 7**(a-c)**). In contrast, the Co16-NA alloy sample retains a predominantly amorphous structure, with no discernible nanocrystalline precipitation (Fig. 7**(**e–g**)**). SAED pattern of the FA sample reveals an additional faint diffraction ring corresponding to the (200) plane (Fig. 7(b)), indicating partial structural transformation under field annealing conditions. Elemental mapping highlights significant differences in element distribution between the two samples. While the Co_{16}-NA alloy shows a uniform elemental distribution with minimal segregation (Fig. 7(h)), the Co_{16}-FA alloy exhibits Cu enrichment within the precipitated phase, accompanied by slight segregation of Fe, Co, Si, and P (Fig. 7(d)). This behavior can be attributed to the large positive mixing enthalpy between Fe and Cu (+13 kJ/mol), which drives the preferential precipitation of Cu, providing heterogeneous nucleation sites for the formation of the α-Fe(Co) nanocrystalline phase. The applied longitudinal magnetic field further promotes this nucleation process, resulting in the formation of a high-density nanocrystalline structure in the FA-treated alloy. According to classical solidification theory, assuming spherical morphology for the secondary phase, the free energy change (ΔG) in the system under an applied magnetic field can be expressed as [53,54]:

$$\Delta G = \frac{4}{3}\pi r^3\left[\Delta G_V + \frac{1}{2}(\mu_2 - \mu_1)H^2\right] + 4\pi r^2\sigma \tag{1}$$

Where ΔG_V is the reduction in free energy per unit volume upon amorphous-to-crystalline transformation, r is the radius of the precipitated nanocrystalline, H is the applied magnetic field strength, σ is the increase of interfacial energy per unit area between the amorphous matrix and the nanocrystalline phase, and μ_1 and μ_2 are the magnetic permeabilities of the amorphous and nanocrystalline phases, respectively. At the critical nucleation point ($d\Delta G/dr=0$), the critical nucleation energy (ΔG^*) and critical radius (r^*) are given by:

$$\Delta G^* = \frac{16\pi\sigma^3}{3\left[|\Delta G_V| + \frac{1}{2}(\mu_2 - \mu_1)H^2\right]^2} \tag{2}$$

$$r^* = \frac{2\sigma}{|\Delta G_V| + \frac{1}{2}(\mu_2 - \mu_1)H^2} \tag{3}$$

It follows that both ΔG^* and r^* are influenced by the magnetic field strength and the difference in permeability between the two phases. Since $\mu_2 > \mu_1$ in the FA sample, so the magnetic field lowers the nucleation energy barrier (ΔG^*) and reduces the critical nucleation radius (r^*), thereby facilitating the amorphous-to-nanocrystalline transformation. Thus, the Co_{16}-FA alloys exhibit a high-density, ultrafine nanocrystalline microstructure compared to its NA-treated counterpart, owing to the applied magnetic field enhancing the nanocrystalline nucleation while suppressing excessive grain growth through competitive growth dynamics and inhibited element diffusion. This refinement in microstructure significantly reduces grain size, resulting in superior soft magnetic properties, making the Co_{16}-FA alloys an excellent candidate for advanced magnetic applications.

Spontaneous magnetization leads to the formation of magnetic domains. To elucidate the origin of magnetic property changes induced by NA and FA treatments in alloys with varying Co contents, the magnetic structure and magnetization process were examined in Fig. 8. Presents the magnetic domain structures of AQ, NA-treated and FA-treated Co_0, Co_8 and Co_{16} samples in the demagnetized state. In the AQ samples, Co_0, Co_8, and Co_{16} alloys all exhibited disordered, irregular domain configurations characterized by uniform domain walls, sharp corners, and multiple forked structures, indicative of strong pinning effects. Narrow, fingerprint-like labyrinthine domains, which are characteristic of stress-induced stripe domains, are prominent amongst Co_0, Co8 and Co16 samples, reflecting internal stress introduced during the manufacturing process. These magnetic domain features suggest the coexistence of in-plane and perpendicular magnetic anisotropies, resulting from the interplay between magnetostriction and residual stress, which ultimately deteriorates the soft magnetic properties, as confirmed by the magnetic performance trends in Fig. 3. Upon NA treatment, the stress-induced stripe domains observed in the AQ samples are largely eliminated, indicating that the annealing process effectively reduces internal stress. Additionally, the domain structure becomes more organized, evolving into wide strip domains. However, residual pinning effects persist, particularly in Co_8 and Co_{16} alloys, as evidenced by the presence of sharp corners and multi-forked domain walls. These observations suggest that while NA treatment improves magnetic softness by partially relieving internal stress, the persistence of domain irregularities and residual pinning effects limits the overall performance enhancement. In contrast, the FA treatment, which applies a longitudinal magnetic field, yields a highly ordered domain structure. The magnetic domains align closely with the external field direction, and the domain width exceeds 200 μm. The domain walls are smooth and free from visible pinning effects, reflecting a significant refinement of the nanocrystalline domain structure. The alignment and stability of these domains, achieved through FA treatment, minimize structural defects and internal stresses, leading to substantial improvements in soft magnetic properties. These findings highlight the critical role of FA treatment in enhancing the magnetic performance of Fe-Co-based alloys by promoting defect-free domain structures and optimizing domain orientation.

The domain structure of AQ, NA-treated and FA-treated Co16 alloys was observed under varying external magnetic fields to correlate the magnetic domain behavior with soft magnetic properties. Fig. 9 illustrates the evolution of domain structures for each treatment as a function of the applied magnetic field. In the AQ samples (Fig. 9(a)), the domains exhibit scattered and irregular distributions at low applied fields due to substantial internal stress and pinning effects. These samples display characteristic stress-induced stripe domains, indicative of magnetostrictive coupling with internal stress. As the external magnetic field increases, the domain walls shift slowly and rotate uniformly. However, the AQ samples show limited sensitivity to field changes and achieve full magnetization when the positive magnetic field reaches 6.5 kA/m. This behavior highlights the significant internal resistance obstructing the alignment of domains with the applied field, resulting in poor soft magnetic performance. In comparison, the NA-treated samples (Fig. 9(b)) exhibit a reduction in internal stress, as evidenced by the disappearance of stress stripe domains. However, pinning effects persist, hindering domain wall movement. As the applied field increases, the domain walls shift incrementally, constrained by residual pinning sites, resulting in gradual and uneven domain transformations. Complete magnetization in the NA samples is achieved at 1.5 kA/m, which is notably lower than that required for the AQ samples (6.5 kA/m). This reduction in magnetization field indicates that while NA treatment alleviates internal stress, the presence of pinning points continues to limit magnetic performance. In contrast, the FA-treated samples (Fig. 9(c)) demonstrate a highly regular domain structure aligned along the direction of the applied magnetic field, with straight and smooth domain

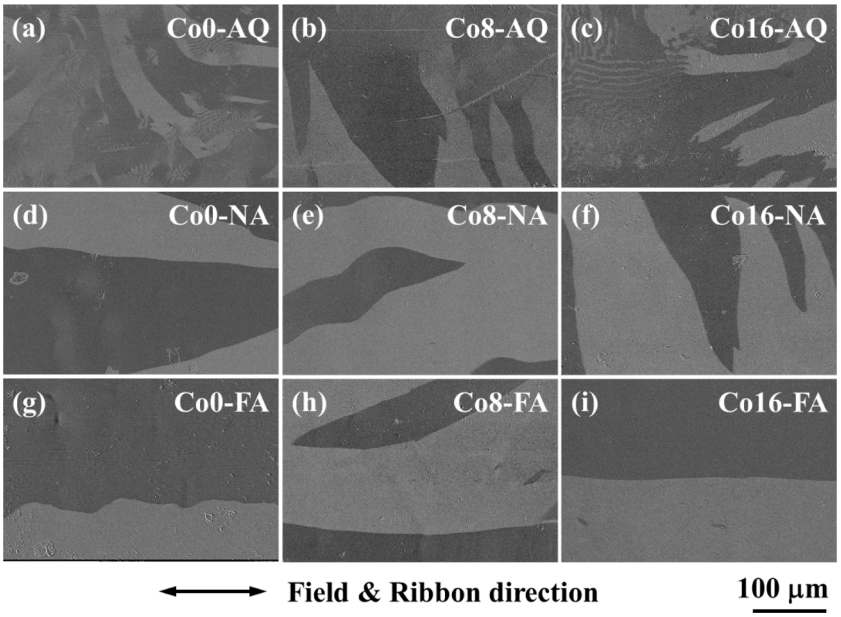

Fig. 8. Magnetic domain images in the demagnetized state of $Fe_{83.2-x}Co_xSi_{2.5}B_{9.5}P_4Cu_{0.8}$ (x = 0, 8, 16) alloys under AQ, NA and FA states.

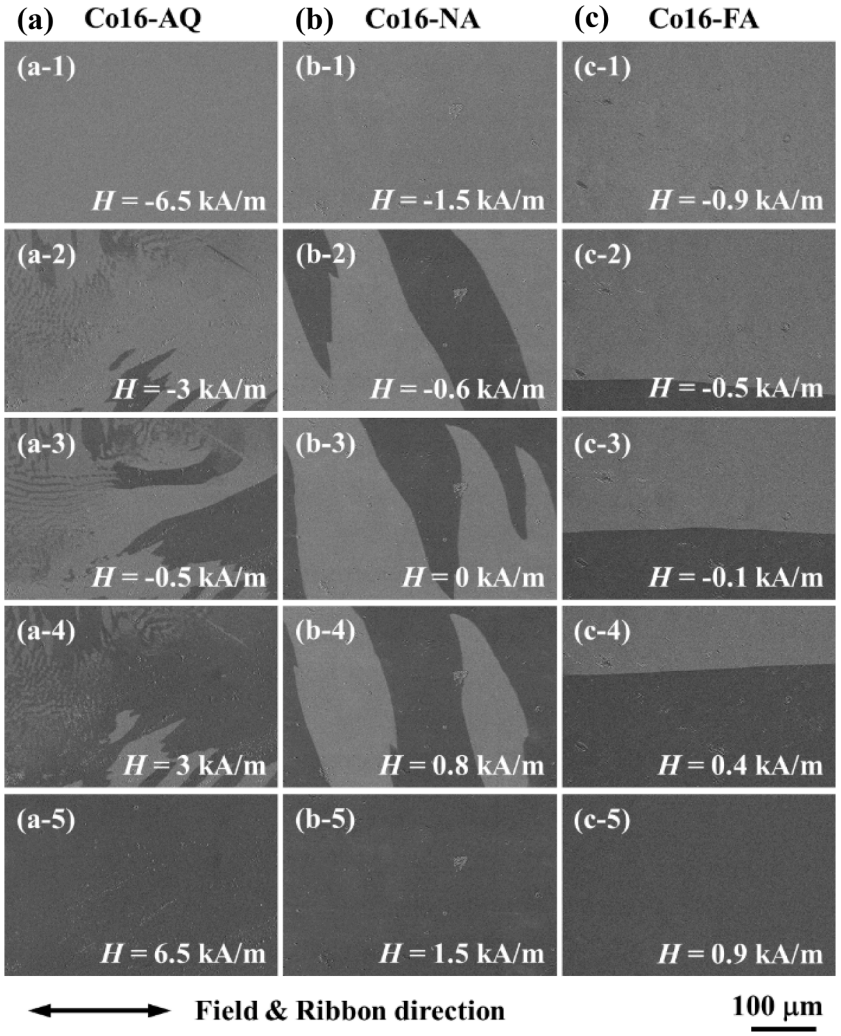

Fig. 9. Magnetic domain evolution of $Fe_{67.2}Co_{16}Si_{2.5}B_{9.5}P_4Cu_{0.8}$ alloy under AQ, NA and FA states during the magnetization process.

walls. The domain widths, exceeding 200 μm, are considerably larger than those in NA-treated samples, reflecting the significant structural refinement achieved through FA treatment. Furthermore, the FA samples are fully magnetized at a much lower field of 0.9 kA/m, indicating minimal internal stress and pinning effects. This reduction in magnetization resistance underscores the effectiveness of FA treatment in enhancing magnetic properties by eliminating structural defects and promoting domain alignment with the applied magnetic field.

Magnetic anisotropy is a key factor affecting the magnetic domain distribution and soft magnetic properties, and the magnetic anisotropy of nanocrystalline alloys mainly includes magnetocrystalline anisotropy, magnetoelastic anisotropy, and magnetic field/stress-induced anisotropy [55]. For FA and NA $Fe_{83.2-x}Co_xSi_{2.5}B_{9.5}P_4Cu_{0.8}$ (x = 0, 4, 8, 12, and 16 at %) nanocrystalline alloys, the extremely low saturation magnetostriction coefficient [24] and the elimination of internal stresses brought about by the high-temperature heat treatment make the magnetoelastic anisotropy basically negligible. In addition, the external stresses have not been introduced during the heat treatment process, so the stress-induced anisotropy is unconsidered. Therefore, the magnetic field induced anisotropy and its interaction with random magnetocrystalline anisotropy and local induced anisotropy should be analyzed.

To estimate the values of K_u, the initial magnetization curves were measured transversal to the ribbon axis of the NA/FA treated Co0, Co8, and Co16 samples and corrected for the demagnetization effects [56]. As shown in Fig. 10, compared to the NA samples, the magnetization curves of FA treated alloys show a significantly linear behavior and reach magnetic saturation at higher magnetic fields, indicating that the magnetization process is dominated by coherent magnetization rotation and that the magnetic field heat treatment produces a homogeneous uniaxial magnetic anisotropy along with a longitudinal susceptible magnetization axis. By extrapolating the initial slop, the K_u is calculated as the area between the magnetization curves of NA and FA samples. [57]. The K_u values of Co0, Co8, and Co16 samples are 183, 213, and 251 J/m^3, respectively, and the corresponding values of magnetic anisotropy field H_k are confirmed to be 226, 258, and 297 A/m.

Based on the average anisotropy model developed by Herzer et al. [58], the average anisotropy constant $<K>$ of a coupled multiphase system, where individual anisotropies are randomly oriented at a scale smaller than the magnetic correlation length, can be expressed as:

$$\langle K \rangle \approx K_u + \frac{1}{2} v_{cr} \sqrt{\beta |K_1| K_u} (D/L_0)^3 \quad (4)$$

where K_1 is the magneto-crystalline anisotropy, K_u denotes induced anisotropy, v_{cr} is crystalline volume fraction, D is the grain size, L_0 is the magnetic correlation length, and β reflects the symmetry of the random anisotropy axes. When the sample is subjected to magnetic field heat treatment, the magnetic field-induced anisotropy K_u is much larger than the average magneto-crystalline anisotropy $<K_1>$ [59], so that the most magnetization-prone axes of each exchange-coupled region rotate in the direction of K_u prone magnetization axis [60], leading to the formation of wide size magnetic domains and their regular arrangement along the K_u direction. The overall K_u of the nanocrystalline alloys mainly originates from the local K_u contribution of the α-(Fe, Co) nanocrystallized phases, which may be caused by the change of crystal symmetry brought about by the directional arrangement of atom pairs of the replacement atom Co and the directional ordering arrangement of the interstitial B atoms [61]. It can be inferred that the compositional and microstructural differences between the Co0 FA, Co8 FA and Co16 FA samples together contribute to the K_u differences. As K_u increases, the differences in the orientation of the easiest magnetization axes between the exchange-coupled regions are smoothed more effectively. As a result, the Co16 FA sample has the smallest local magnetic inhomogeneity compared to the Co0 FA and Co8 FA samples.

When magnetization is governed by long-range anisotropies and their coupling exceeds the exchange length, the H_c is determined by anisotropy fluctuations δ_K and can be described by:

$$H_c \approx \frac{1}{2J_s} \left| \overline{\frac{\partial \gamma_W}{\partial x}} \right|_{max} \approx \frac{\delta K}{J_s} \frac{L_{ex}}{l_k} \quad (5)$$

where γ_w is the domain wall energy, L_{ex} is the exchange length and l_k represents the fluctuation length of the effective anisotropy. In FA samples, where the grain size D is significantly smaller than exchange length L_{ex}, and the coercivity is proportional to the anisotropy fluctuation $H_c \propto \delta K/J_s$. The magnetic permeability μ depends on the angle between the applied magnetic field and the macroscopic anisotropy direction. When the magnetization direction aligns with the induced anisotropy K_u, permeability is controlled by domain wall pinning, with $\mu \propto 1/\delta_K$. Co16 FA samples have the smallest local magnetic inhomogeneity and thus the smallest anisotropic fluctuation, the smallest coercivity, and thus the best soft magnetic properties.

4. Conclusion

This study elucidates the synergistic effects of Co substitution and longitudinal magnetic field annealing (FA) on the microstructure, magnetic domain behavior, and soft magnetic properties of $Fe_{83.2-x}Co_xSi_{2.5}B_{9.5}P_4Cu_{0.8}$ (x = 0, 4, 8, 12, 16) alloys. Our findings demonstrate that FA treatment is a powerful strategy for inducing high-density nanocrystal nucleation and inhibits excessive grain growth by constraining element diffusion, yielding a refined microstructure with superior magnetic softness. The transition from non-uniform magnetic domain rotation to uniform domain wall displacement further enhances the magnetic properties. Among the alloys investigated, the $Fe_{67.2}Co_{16}Si_{2.5}B_{9.5}P_4Cu_{0.8}$ composition exhibits remarkable soft magnetic performance, achieving a B_s of 1.85 T, an ultra-low H_c of 1.8 A/m, and an exceptional μ_e of 26,505 at 1 kHz. Moreover, the core loss of the FA-treated alloy is significantly reduced, ensuring high magnetic efficiency across a wide range of operating conditions. These results position FA-treated Fe-Co-based nanocrystalline alloys as promising

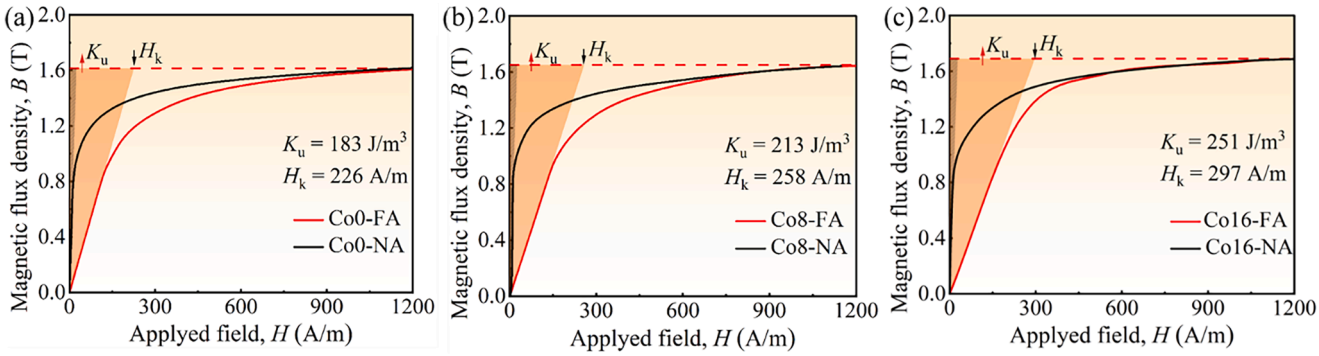

Fig. 10. Initial magnetization curves measured transversally and demagnetization effect of (a) Co0-NA/FA, (b) Co8-NA/FA and (c) Co16-NA/FA samples.

candidates for energy-efficient applications, such as high-performance transformers and electric motors.

Data availability

Data will be made available on request.

CRediT authorship contribution statement

Mufeng Jiang: Writing – original draft, Methodology, Investigation. **Jingjing Wang:** Writing – original draft, Methodology, Investigation. **Mingjuan Cai:** Data curation. **Jun Li:** Methodology. **Wanying Dong:** Data curation. **Zhijun Guo:** Writing – review & editing, Methodology, Conceptualization. **Baolong Shen:** Methodology, Funding acquisition, Conceptualization.

Declaration of competing interest

The authors declare that they have no known competing financial interests or personal relationships that could have appeared to influence the work reported in this paper.

Acknowledgments

This work was financially supported by the National Key R&D Program of China (No. 2022YFB3804100), the National Natural Science Foundation of China (No. 52231005), the Jiangsu Provincial Key R&D Program (No. BE2021088), and the Start-up Research Fund of Southeast University (No. RF1028623113).

References

[1] J.M. Silveyra, E. Ferrara, D.L. Huber, T.C. Monson, Soft magnetic materials for a sustainable and electrified world, Science 362 (2018) eaao0195.
[2] B. Sai Ram, A.K. Paul, S.V. Kulkarni, Soft magnetic materials and their applications in transformers, J. Magn. Magn. Mater. 537 (2021) 168210.
[3] H.X. Li, Z.C. Lu, S.L. Wang, Y. Wu, Z.P. Lu, Fe-based bulk metallic glasses: glass formation, fabrication, properties and applications, Prog. Mater Sci. 103 (2019) 235–318.
[4] G.Y. Ouyang, B. Jensen, W. Tang, J. Schlagel, B. Hilliard, C.C. Pan, B.Z. Cui, K. Dennis, D. Jiles, T. Monson, I. Anderson, M.J. Kramer, J. Cui, Near net shape fabrication of anisotropic Fe-6.5%Si soft magnetic materials, Acta Mater. 201 (2020) 209–216.
[5] T.N. Lamichhane, L. Sethuraman, A. Dalagan, H. Wang, J. Keller, M. P. Paranthaman, Additive manufacturing of soft magnets for electrical machines - a review, Mater. Today Phys. 15 (2020) 100255.
[6] A. Inoue, F. Kong, Soft Magnetic Materials, Encyclopedia of Smart Materials. English, America, 2022, pp. 10–23.
[7] C. Suryanarayana, A. Inoue, Iron-based bulk metallic glasses, Int. Mater. Rev. 58 (2013) 131–166.
[8] M.A. Willard, M. Daniil, K.E. Kniping, Nanocrystalline soft magnetic materials at high temperatures: a perspective, Scr. Mater. 67 (2012) 554–559.
[9] Y. Yoshizawa, S. Oguma, K. Yamauchi, New Fe-based soft magnetic alloys composed of ultrafine grain structure, J. Appl. Phys. 64 (1988) 6044–6046.
[10] P. Sharma, X. Zhang, Y. Zhang, A. Makino, Competition driven nanocrystallization in high B_s and low coreloss Fe-Si-B-P-Cu soft magnetic alloys, Scr. Mater. 95 (2015) 3–6.
[11] H. Li, A.D. Wang, T. Liu, P.B. Chen, A.N. He, Q. Li, J.H. Luan, C.T. Liu, Design of Fe-based nanocrystalline alloys with superior magnetization and manufacturability, Mater. Today 42 (2021) 49–56.
[12] Y.H. Li, X.J. Jia, W. Zhang, Y. Zhang, G.Q. Xie, Z.Y. Qiu, J.H. Luan, Z.B. Jiao, Formation and crystallization behavior of Fe-based amorphous precursors with pre-existing α-Fe nanoparticles—Structure and magnetic properties of high-Cu-content Fe-Si-B-Cu-Nb nanocrystalline alloys, J. Mater. Sci. Technol. 65 (2021) 171–181.
[13] L. Hou, X.D. Fan, Q.Q. Wang, W.M. Yang, B.L. Shen, Microstructure and soft-magnetic properties of FeCoPCCu nanocrystalline alloys, J. Mater. Sci. Technol. 35 (2019) 1655–1661.
[14] Q. Luo, D.H. Li, M.J. Cai, S.Y. Di, Z.G. Zhang, Q.S. Zeng, Q.Q. Wang, B.L. Shen, Excellent magnetic softness-magnetization synergy and suppressed defect activation in soft magnetic amorphous alloys by magnetic field annealing, J. Mater. Sci. Technol. 116 (2022) 72–82.
[15] C.L. Zhao, A.D. Wang, A.N. He, C.T. Chang, C.T. Liu, Nano-heterogeneity-stabilized and magnetic-interaction-modulated metallic glasses, Sci. China Mater. 64 (2021) 1813–1819.
[16] T. Suetsuna, H. Kinouchi, N. Sanada, Roles of cobalt and boron in FeCoBSi soft magnetic composite with in-plane uniaxial magnetic anisotropy, J. Magn. Magn. Mater. 519 (2021) 167475.
[17] T. Liu, F.Y. Kong, L. Xie, A.D. Wang, C.T. Chang, X.M. Wang, C.T. Liu, Fe(Co) SiBPCCu nanocrystalline alloys with high Bs above 1.83 T, J. Magn. Magn. Mater. 441 (2017) 174–179.
[18] Y.H. Li, Z.M. Wang, W. Zhang, Minor-Cu doped soft magnetic Fe-based FeCoBCSiCu amorphous alloys with high saturation magnetization, AIP Adv. 8 (2018) 056115.
[19] X.Y. Duan, Y.H.Li S.W.Ju, Z.W. Zhu, H.F. Zhang, W. Zhang, Effects of B/P and Co/Fe substitutions on glass-forming ability and soft magnetic properties of a $Fe_{80}P_{13}C_7$ metallic glass, J. Non Cryst. Solids 616 (2023) 122480.
[20] X.J. Jia, W. Zhang, Y.Q. Dong, J.W. Li, A.N. He, J.H. Luan, R.W. Li, Unusual alloying effects of Co and Ni on structure and magnetic properties of Fe-Si-B-Cu nanocrystalline alloys with pre-existing α-Fe nanocrystals, J. Alloys Compd. 920 (2022) 166030.
[21] A. Williams, V. Moruzzi, A. Malozemoff, K. Terakura, Generalized Slater-Pauling curve for transition-metal magnets, IEEE Trans. Magn. 19 (1983) 1983–1988.
[22] K.A. Gallagher, M.A. Willard, V.N. Zabenkin, D.E. Laughlin, M.E. McHenry, Distributed exchange interactions and temperature dependent magnetization in amorphous $Fe_{88-x}Co_xZr_7B_4Cu_1$ alloys, J. Appl. Phys. 85 (1999) 5130–5132.
[23] J. Jia, L. Shi, Y. Wu, R. Wang, W. Guo, Y. Shao, N. Chen, K. Yao, Effect of Sn, Bi and In on the magnetic properties and microstructure of Fe-B-C-Si-P-Cu-M nanocrystalline alloys, J. Non Cryst. Solids 647 (2025) 123277.
[24] J. Hu, S. Bao, Y. Cheng, C. Liu, Y. Zhao, Y. Liu, J. Chang, Improving the amorphous forming ability of FeSiBPCu nanocrystalline alloys by substituting Cu with C, J. Non Cryst. Solids 648 (2025) 123313.
[25] W. Zhang, R. Li, J. Wang, T. Zhang, Y. Gao, T. Zhang, Tailoring microstructure in a soft-magnetic Fe-based amorphous-nanocrystalline alloy for high resistivity according to electrical percolation threshold, Mater. Des. 246 (2024) 113311.
[26] Q. Zhang, Y. Meng, C. Zhao, C. Chang, S. Pang, S. Zhou, Rapid-annealed FeSiBPCu nanocrystalline alloy with high B_s approaching 1.9 T and good bendability, J. Mater. Res. Technol. 33 (2024) 5204–5209.
[27] S. Tang, R. Sun, Y. He, G. Liu, R. Wang, Y. Liu, C. Tang, Machine learning assisted design and preparation of $Fe_{85}Si_2B_{8.5}P_{3.5}C_1$ amorphous/nanocrystalline alloy with high B_s and low H_c, Mater. Des. 248 (2024) 113461.
[28] T.X. Huang, Z.B. Song, Q. Yan, L.L. Lu, H.Z. Zhou, A. Jain, Y.G. Wang, Microstructure, thermal stability and soft magnetic properties of $Fe_{81}B_{10}P_8Cu_1$ amorphous/nanocrystalline alloy refined by slags with low basicity, MSEB 308 (2024) 117601.
[29] L. Xie, Q. Li, C. Chang, X. Fan, A. He, Y. Cai, Y. Dong, Influence of P and C co-alloying on soft magnetic properties and crystallization behavior of FeSiBPCCu nanocrystalline alloys, J. Mater. Res. Technol. 33 (2024) 3106–3116.
[30] L. Shi, Y. Shao, J. Jia, C. Lu, K. Yao, Roles of Cu in Fe-based soft magnetic nanocrystalline alloys with high Fe content, Intermetallics 166 (2024) 108202.
[31] G.G. Xi, C. Sun, M.H. Han, H.G. Li, J.L. Cui, T. Zhang, Ultra-high annealing stability via the synergistic homogenization mechanism of Cu-P clusters in Fe-P-based nanocrystalline alloy, J. Non Cryst. Solids 633 (2024) 122951.
[32] Y. Li, N. Shen, J. Zhang, X. Hui, Decreasing the sensitivity of soft magnetic properties to heat-treatment process parameters by minor Nb alloying in $Fe_{83}C_4B_{6.5}P_{5.5}Cu_1$ nanocrystalline alloys, Intermetallics 170 (2024) 108335.
[33] C.R. Wang, Y.H. Li, B.S. Li, L. Jiang, T.C. Liu, W. Zhang, Optimizing structure and magnetic softness of low-Nb-content Fe-Si-B-Nb-Cu nanocrystalline alloys by regulating Si/B ratio and Cu content, Mater. Today Commun. 40 (2024) 110043.
[34] M.Y. Guo, J.S. Xue, Y.H. Li, L. Jiang, L. Qi, Rie Y. Umetsu, W. Zhang, Effects of Cr addition on structure, magnetic properties and corrosion resistance of a $Fe_{85.5}B_{13}Cu_{1.5}$ nanocrystalline alloy, J. Mater. Res. Technol. 30 (2024) 2902–2910.
[35] L.C. Wu, Y.H. Li, A.N. He, Z.W. Zhu, H.F. Zhang, W. Zhang, Improvement of soft magnetic properties of a nanoperm-type Fe-Hf-B nanocrystalline alloy upon surface crystallization inhibition by Cu addition, Intermetallics 163 (2023) 108040.
[36] C.C. Cao, L. Zhu, Y. Meng, X.B. Zhai, Y.G. Wang, Atomic level structural modulation during the structural relaxation and its effect on magnetic properties of $Fe_{81}Si_4B_{10}P_4Cu_1$ nanocrystalline alloy, J. Magn. Magn. Mater. 456 (2018) 274–280.
[37] M. Kuhnt, M. Marsilius, T. Strache, C. Polak, G. Herzer, Magnetostriction of nanocrystalline (Fe,Co)-Si-B-P-Cu alloys, Scr. Mater. 130 (2017) 46–48.
[38] M. Ohta, Y. Yoshizawa, Magnetic properties of nanocrystalline $Fe_{82.65}Cu_{1.35}Si_xB_{16-x}$ alloys (x=0-7), Appl. Phys. Lett. 91 (2007) 062517.
[39] P. Sharma, X. Zhang, Y. Zhang, A. Makino, Influence of microstructure on soft magnetic properties of low coreloss and high B_s $Fe_{85}Si_2B_8P_4Cu_1$ nanocrystalline alloy, J. Appl. Phys. 115 (2014) 17A304.
[40] X.J. Jia, Y.H. Li, L.C. Wu, W. Zhang, Structure and soft magnetic properties of Fe-Si-B-P-Cu nanocrystalline alloys with minor Mn addition, AIP Adv. 8 (2018) 056110.
[41] Y.H. Li, Z.M. Wang, W. Zhang, Minor-Cu doped soft magnetic Fe-based FeCoBCSiCu amorphous alloys with high saturation magnetization, AIP Adv. 8 (2018) 056115.
[42] R. Parsons, K. Suzuki, Nanocrystalline soft magnetic materials produced by continuous ultra-rapid annealing (CURA), AIP Adv. 12 (2022) 035316.
[43] K. Suzuki, R. Parsons, B. Zang, K. Onodera, H. Kishimoto, A. Kato, Copper-free nanocrystalline soft magnetic materials with high saturation magnetization comparable to that of Si steel, Appl. Phys. Lett. 110 (2017) 012407.
[44] X.J. Jia, Y.H. Li, L.C. Wu, W. Zhang, A study on the role of Ni content on structure and properties of Fe-Ni-Si-B-P-Cu nanocrystalline alloys, J. Alloys Compd. 822 (2022) 152784.

[45] Y.H. Li, X.J. Jia, Y.Q. Xu, C.T. Chang, G.Q. Xie, W. Zhang, Soft magnetic Fe-Si-B-Cu nanocrystalline alloys with high Cu concentrations, J. Alloys Compd. 722 (2017) 859–863.
[46] Z. Li, R. Parsons, H. Kishimoto, T. Shoji, A. Kato, J. Karel, K. Suzuki, Nanocrystalline $(Fe,Co,Ni)_{86}B_{14}$ soft magnetic alloys prepared by ultra-rapid annealing, J. Alloys Compd. 902 (2022) 162554.
[47] W.D. Lin, Y.Z. Yang, J. Xu, W. Li, Effect of Nb, Si and Cu on the crystallization process and magnetic properties of FeNbBP alloys, J. Alloys Compd. 735 (2018) 1195–1199.
[48] Z. Xiang, A.D. Wang, C.L. Zhao, H. Men, X.M. Wang, C.T. Chang, D. Pan, Optimization of thermal stability and soft-magnetic properties of FeSiBPCuNb alloys by Nb content tuning, J. Alloys Compd. 622 (2015) 1000–1004.
[49] J. Xu, X. Liu, Y.F. Wang, G.T. Wang, J. Wang, L. Zhou, Y.Z. Yang, Nanocrystallization, magnetic properties and bending ductility of antiferromagnetic Mn-doped FeSiBCuPC alloys induced by micro-compressive stress annealing, J. Alloys Compd. 882 (2021) 160746.
[50] H. Zheng, L. Zhu, S.S. Jiang, Y.G. Wang, S.N. Liu, S. Lan, F.G. Chen, Role of Ni and Co in tailoring magnetic and mechanical properties of $Fe_{84}Si_2B_{13}P_1$ metallic glass, J. Alloys Compd. 816 (2020) 152549.
[51] L.X. Jiang, Y. Zhang, X. Tong, T. Suzuki, A. Makino, Unique influence of heating rate on the magnetic softness of $Fe_{81.5}Si_{0.5}B_{4.5}P_{11}Cu_{0.5}C_2$ nanocrystalline alloy, J. Magn. Magn. Mater. 471 (2019) 148–152.
[52] J. Xu, Y.Z. Yang, Q.S. Yan, G.H. Xiao, T. Luo, C.F. Fan, Softening and magnetic properties of ultrahigh Fe content FeSiBCuPC nanocrystalline alloy induced by low-pressure stress annealing, Scr. Mater. 179 (2020) 6–11.
[53] Y.X. Zhuang, J. Chen, W.J. Liu, J.C. He, Effect of high magnetic field on crystallization of $Zr_{46.75}Ti_{8.25}Cu_{7.5}Ni_{10}Be_{27.5}$ bulk metallic glass, J. Alloys Compd 504 (2010) S256–S259.
[54] X.-d Wang, M. Qi, S. Yi, Crystallization behavior of bulk amorphous alloy $Zr_{62}Al_8Ni_{13}Cu_{17}$ under high magnetic field, Scr. Mater. 51 (2004) 1047–1050.
[55] S. Flohrer, R. Schäfer, C. Polak, G. Herzer, Interplay of uniform and random anisotropy in nanocrystalline soft magnetic alloys, Acta Mater. 53 (2005) 2937–2942.
[56] J.S. Blázquez, J. Marcin, F. Andrejka, V. Franco, A. Conde, I. Skorvanek, Anisotropy field distribution in soft magnetic Hitperm alloys submitted to different field annealing processes, J. Alloys Compd. 658 (2016) 367–371.
[57] L.K. Varga, Z. Gercsi, G. Kovács, A. Kákay, F. Mazaleyrat, Stress-induced magnetic anisotropy in nanocrystalline alloys, J. Magn. Magn. Mater. 254-255 (2003) 477–479.
[58] G. Herzer, Modern soft magnets: amorphous and nanocrystalline materials, Acta Mater. 61 (2013) 718–734.
[59] A. He, J. Li, M. Wang, A. Wang, Y. Xiao, Y. Dong, H. Guo, R. Jiang, W. Xia, L. Dong, H. Wang, J. Ge, Microstructure, magnetic domain and dynamic loss of surface-textured Fe-based nanocrystalline alloy, J. Mater. Sci. Technol. 120 (2022) 1–7.
[60] S. Flohrer, G. Herzer, Random and uniform anisotropy in soft magnetic nanocrystalline alloys (invited), J. Magn. Magn. Mater. 322 (2010) 1511–1514.
[61] K. Suzuki, G. Herzer, Magnetic-field-induced anisotropies and exchange softening in Fe-rich nanocrystalline soft magnetic alloys, Scr. Mater. 67 (2012) 548–553.